Rare Metal Materials and Engineering
Volume 54, Issue 8, August 2025
Available online at www.rmme.ac.cn

Science Press

Cite this article as: Chu Qingquan, Hou Xingyu, Cheng Yin, et al. Influence of Casting Defects on Weldability of a Nickel-Based Superalloy[J]. Rare Metal Materials and Engineering, 2025, 54(08): 1917-1925.
DOI: https://doi.org/10.12442/j.issn.1002-185X.20240423.

ARTICLE

Influence of Casting Defects on Weldability of a Nickel-Based Superalloy

Chu Qingquan[1,2], Hou Xingyu[1], Cheng Yin[1], Qin Jian[3], Wang Shiyang[1], Sun Yuan[1], Sun Xiaofeng[1]

[1] Shi-changxu Innovation Center for Advanced Materials, Institute of Metal Research, Chinese Academy of Sciences, Shenyang 110016, China; [2] School of Materials Science and Engineering, University of Science and Technology of China, Shenyang 110016, China; [3] State Key Laboratory of Advanced Brazing Metals & Technology, Zhengzhou Research Institute of Mechanical Engineering Co., Ltd, China Academy of Machinery Science and Technology, Zhengzhou 450052, China

Abstract: The impact of casting defects on the weldability of K4951 superalloy was investigated using tungsten inert gas (TIG) welding. The as-cast K4951 superalloy samples with prefabricated U-shaped grooves of varying depths and widths were TIG welded, and the microstructures, cracks morphology, and precipitated phases were analyzed using optical microscope, scanning electron microscope, transmission electron microscope, and energy dispersive X-ray spectrometer. The results reveal that the dimensions of casting defects significantly affect the weldability of K4951. Deep defects (greater than 2 mm) lead to rapid crack propagation, while wider defects can moderate the propagation process of cracks. Elemental segregation and the formation of precipitated phases, such as *M*C carbides, are observed in the fusion zone, contributing to welding cracks. An optimal groove aspect ratio (depth-to-width) between 0.2 and 0.5 minimizes crack formation tendency and enhances tensile strength, resulting in a mixed brittle-ductile fracture mode of joint after high-temperature tensile testing.

Key words: casting defect; K4951; TIG; weldability

1 Introduction

Superalloys based on Fe, Co, or Ni exhibit excellent resistance to high-temperature oxidation and creep, and maintain structural stability, playing an essential role in aerospace, petrochemical, nuclear power, and other fields[1–3]. K4951 is a polycrystalline nickel-based superalloy characterized by low density, high melting point, and low content of rare-earth elements. It possesses excellent resistance to oxidation and thermal fatigue, making it suitable for aero-engine components, such as floating tiles in combustion chambers and turbine guide vanes[4–9].

Most of the structural components of superalloys are fabricated by casting methods. Nickel-based superalloys contain various alloying elements and have a broad solidification temperature range, resulting in the development of pronounced dendrites during the casting process. These interconnected dendrites impede the flow of liquid metal, and upon cooling, they result in numerous dispersed casting defects, such as shrinkage pore. Hot isostatic pressing (HIP) and welding techniques can repair the defects generated in the casting process. HIP effectively repairs holes and microstructural damage, thereby significantly enhancing mechanical properties[10–11]. However, its capability to repair surface defects on castings is restricted. Conversely, welding technique is irreplaceable for repairing surface defects and damage, as well as connecting different components of the casting[12–14].

Received date: July 15, 2024
Foundation item: National Natural Science Foundation of China (52201054, 52175368); National Science and Technology Major Projects (J2019-VI-0018-0133); Liaoning Provincial Science and Technology Program (2023-BS-019, 2023-MS-020); National Key R&D Program of China (2021YFB3700401); Key Specialized Research and Development Break-Through-Unveiling and Commanding the Special Project Program in Liaoning Province (2021JH15)
Corresponding author: Wang Shiyang, Ph. D., Associate Professor, Institute of Metal Research, Chinese Academy of Sciences, Shenyang 110016, P. R. China, E-mail: sywang16b@imr. ac. cn; Sun Yuan, Ph. D., Professor, Institute of Metal Research, Chinese Academy of Sciences, Shenyang 110016, P. R. China, E-mail: yuansun@imr. ac. cn; Sun Xiaofeng, Ph. D., Professor, Institute of Metal Research, Chinese Academy of Sciences, Shenyang 110016, P. R. China, E-mail: xfsun@imr.ac.cn

Research on the weldability of precipitation-strengthened nickel-based superalloys, such as K4951, where the content of Al and Ti elements exceeds 6%, has always been a challenging issue[15–16]. The high volume fraction of the γ' phase leads to the formation of solidification cracks[17], liquation cracks[18], and ductility-dip cracks[19] during welding, and strain-ageing cracks[20] during the post-weld heat treatment process. Controlling the initiation and propagation of these cracks will significantly expand the application field of welding technique. Tungsten inert gas (TIG) welding has been widely used in superalloy welding repair because of its simple operation, convenience, flexibility, and better welding effect[13,21–22]. By changing the cooling rate of heat treatment before TIG welding, Wen et al[12] promoted the precipitation of the chain-like $M_{23}X_6$ phase at the grain boundary of the welding fusion zone, and improved the weldability of the M951 superalloy. Ariaseta et al[23] eliminated the γ/Laves eutectic in the welded joint and improved the joint performance by changing the post-weld heat treatment temperature of TIG welding for G27 superalloy keyhole.

Currently, most researches focus on the causes of cracks in TIG welding and the improvement of superalloy weldability by changing welding parameters[23–26]. However, there are few researches on the TIG welding's repair ability for casting defects and damage. Rush[27] and Richards[28] et al found a deep connection between the aspect ratio of the molten pool and weld quality, but there is no specific correlation between them. The present research explored the influence of casting defect severity on the weldability of K4951 superalloy using TIG welding to repair various degrees of prefabricated defects. The results will guide appropriate repair methods for different casting defects.

2 Experiment

Cast polycrystalline K4951 superalloy was prepared in a vacuum induction furnace and cast into sheets with 7 mm in thickness. The chemical composition of the K4951 superalloy is listed in Table 1. The welding samples with dimensions of 60 mm×30 mm×6 mm were machined by an electrical discharge machine. Defects are usually circular grooves with different depths and radii. When using welding methods to repair casting defects, it is necessary to grind the defects into long strip grooves to facilitate the transportation of welding wires. The grooves on the welding samples were designed as U-shaped grooves with different depths and widths, aiming to simulate different casting defects in the casting process. The groove diagram is shown in Fig.1, and the groove parameters are shown in Table 2. The welding samples were fusion welded with welding wires by TIG technique, and welding wires, whose composition is similar to K4951, were cut from the as-cast sheets with 1 mm in diameter. The TIG welding

Table 1 Chemical composition of K4951 superalloy (wt%)

Cr	Al	Co	W	Mo	Nb	C	B	Ni
9	6	5	3.5	3	1.8	0.02	0.0014	Bal.

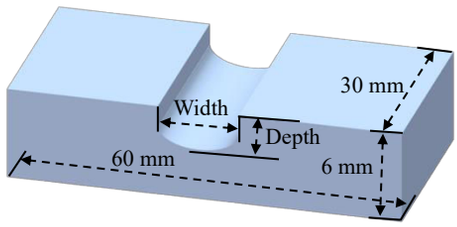

Fig.1 Schematic illustration of K4951 with prefabricated U-shaped groove

Table 2 Parameters of grooves with different depths and widths (mm)

Groove	Depth	Width
G1	1	4
G2	2	4
G3	3	4
G4	3	3
G5	3	5
G6	3	8

was carried out at a welding current of 50 A, a welding voltage of 8.5–9.5 V, a welding speed of 20 mm/min, and a constant distance of 1.5 mm between the electrode tip and the grooves. High-purity argon gas (purity>99.999%) was used as the shielding gas, with a flow rate of 10 mL/min through a copper pipe.

Transverse sections were cut perpendicularly to the welding direction from the welded samples for microstructural characterization using optical microscope (OM, LEICA DMi8), scanning electron microscope (SEM, ZEISS Gemini 300) equipped with an energy dispersive X-ray spectrometer (EDS), transmission electron microscope (TEM, FEI Talos F200X), and selected area electron diffractometer (SAED). The transverse sections were polished and chemically etched in a solution consisting of 40 g $CuSO_4$+200 mL H_2O+200 mL HCl before OM and SEM observations. Besides the non-etched metallography, vibration polishing was used to obtain the elemental composition by electron probe microanalyzer (EPMA, JEOL JXA-lhp200f) and crystal orientation by electron backscattered detection (EBSD). The result of the EBSD was analyzed using AZtecCrystal software. SEM image represented the microstructure morphology of the scanning area, the inverse pole figure (IPF) represented the distribution of crystal orientation, and the kernel average misorientation (KAM) map represented the distribution of dislocation density. The crack statistics in the transverse sections of welding samples were measured using Image Pro Plus 6.0 software. TEM samples were electrolytically thinned using a twinjet in a solution consisting of 10vol% $HClO_4$+90vol% C_2H_5OH at –25 ℃. The Thermo-Calc software with a TCNi10 database was used to calculate the evolution of the equilibrium phases in the K4951 superalloy and the welding wire. The precipitated phase in the transverse sections of

welding samples was determined using the X-ray diffractometer (XRD, Rigaku SmartLab). A tensile test was carried out on the welding samples at 800 ℃, and the fracture morphology was observed to analyze fracture mechanisms.

3 Results and Discussion

3.1 Microstructures of transverse sections of as-welded K4951

The OM microstructures of the as-welded joints with six kinds of grooves are shown in Fig.2. The weld is well formed, and the joint structure is divided into three parts: fusion zone (FZ), heat-affected zone (HAZ), and base metal (BM). The casting dendrite characteristics of K4951 BM are obvious. Remelting and metallurgical bonding occur in the weld zone, and the corrosion effect is not as obvious as that of the BM. Welding cracks are found in the cross-section of each sample, most of which extend from the FZ to the BM. In contrast, a few cracks only sprout and extend macroscopically in the FZ, which are wide and flat and will have a devastating effect on the welded joint. In addition, comparing the results of the six welds, it is observed that the depth of the groove has a greater impact on the weld results than the width of the groove, and when the depth of the groove is greater than 2 mm, the weld cracks are rapidly expanded. By increasing the width of the groove, the cracking is moderated, but the width continues to increase, and the cracks also increase dramatically. The presence of unfused defects at the bottom of some welds may be related to wire metal fluidity, tungsten electrode wear, or incomplete argon gas protection.

The phase composition of the joints with different groove shapes after welding is the same. Taking the groove G2 as an example, the SEM micrographs of corresponding joint are shown in Fig. 3. The FZ changes from columnar crystals in edge to equiaxial crystals center due to the temperature gradient. Compared with the BM area, the morphology of carbides in the FZ is fine and dispersed, and the content of carbides in the HAZ is less. Semi-melted grains and liquefiable carbide particles affected by the welding thermal cycle are observed near the fusion line. The fluctuation of the fusion line also reflects that the temperature bearing capacity of the grain boundary is weaker than that of the grain. In addition, recrystallization is also observed at the boundary of the FZ.

Welding is a rapid melting and solidification process, with a heating and cooling rate of 10^5–10^7 K/m[29], which is a typical non-equilibrium solidification process, and is bound to exist by the redistribution of solutes, element segregation, and uneven precipitation of precipitation strengthening phases. These problems are the root causes of welding cracks. The elements segregation in the FZ of the joints with six kinds of groove shapes is analyzed by EPMA, and the results are shown in Fig. 4. The calculation formula of segregation coefficient K[30] is as follows:

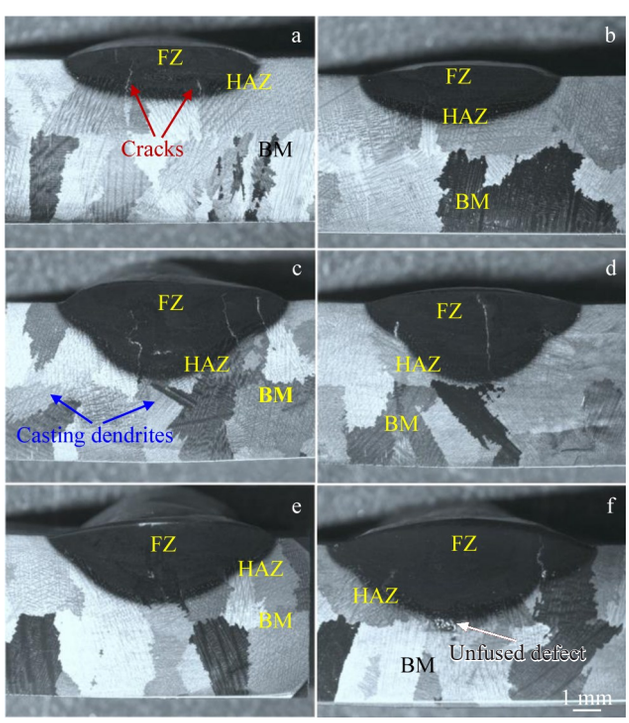

Fig.2 OM images of joints with six kinds of grooves: (a) G1; (b) G2; (c) G3; (d) G4; (e) G5; (f) G6

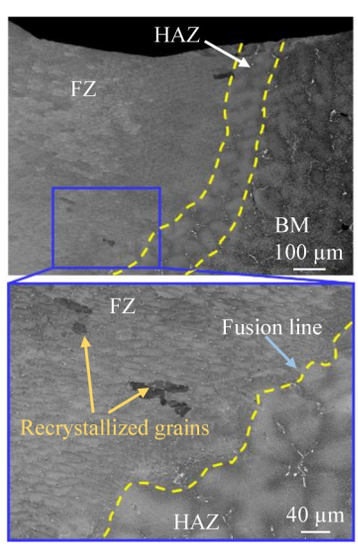

Fig.3 SEM microstructures of the joint with groove G2

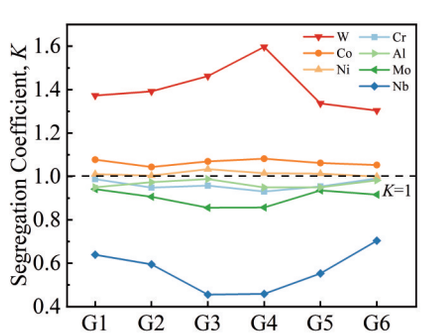

Fig.4 Segregation of elements in the joints with six kinds of grooves

$$K=\frac{C_d}{C_{id}} \quad (1)$$

where C_d is the content of an element in the dendrite of the FZ; C_{id} is the content of an element in the interdendritic of the FZ. $K>1$ indicates that the elements are concentrated in the dendrite, otherwise, the elements are concentrated in the interdendritic area. In the FZ, elements W, Co, and Ni are segregated in the dendrites, and elements Cr, Al, Mo, and Nb are segregated in the interdendritic area. The segregation degree of elements W and Nb is the largest in the dendrite and interdendritic area. The degree of element segregation is the largest in joints with grooves G3 and G4, and is the smallest in joints with grooves G1 and G6.

The simulation result of the equilibrium solidification process of the weld is shown in Fig. 5a. The result shows that the K4951 superalloy weld mainly contains γ, γ', MC carbides, and M_3B_2 borides during the solidification process, which is consistent with the results of the study on the precipitated phase of K4951 superalloy by Lian et al[31]. The XRD patterns for the six joints with different groove shapes, as shown in Fig. 5b, are not significantly different from the corresponding calculation results. MC carbides are mainly NbC, and there is no boride. It is considered that the precipitation of boride is less, and the accuracy of XRD analysis is insufficient.

The precipitated phases in the FZ of the joints with six different groove shapes are mainly chain-like, granular, and granular phase groups composed of fine granular phases. The SEM and EDS results of these precipitated phases are shown in Fig. 6. The size of these precipitated phases is within 1 μm and rich in elements Nb and Mo. The TEM images of the precipitated phase are shown in Fig. 7. The precipitated phases with different morphologies have the same lattice structure. EDS results indicate that the precipitated phase is $Ni_{11}Nb_{56}Mo_{10}C_{18}Cr_5$ (at%), so it is judged that the precipitated phases of the FZ are nano-scale MC carbides.

3.2 Crack morphology and formation reasons of joints

Two primary types of welding cracks, solidification crack, and liquation crack are mainly found in the weld of the joints

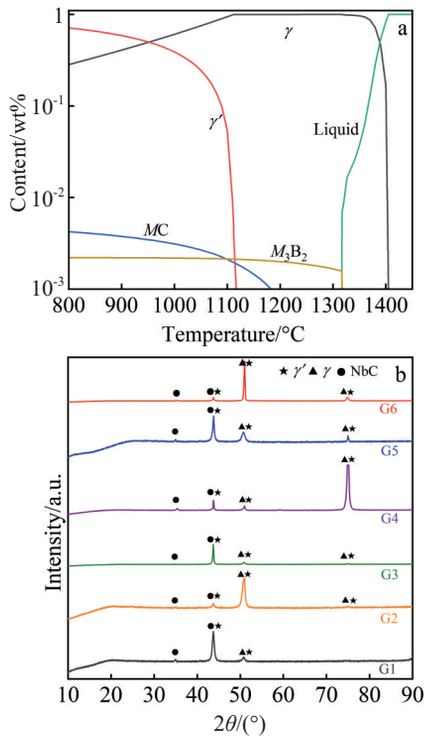

Fig.5 Equilibrium phase diagram of the K4951 superalloy calculated by Thermal Calc (a); XRD patterns of the joints with six kinds of groove shapes (b)

with six kinds of groove shapes. Solidification cracks are predominantly found in the FZ, where high volume fractions of solid phase during the final stages of weld solidification restrict liquid metal reflux to fill the interdendritic area, as well as the bias of low melting point elements towards the grain boundaries to form a low-melting-point liquid film, which leads to cracking of the alloy under the ensuing thermal stress[17,32]. Most solidification cracks are relatively straight, cracking along the intergranular direction, and the crack length and width are larger than those of other cracks. The solidification crack morphology is shown in Fig. 8. The

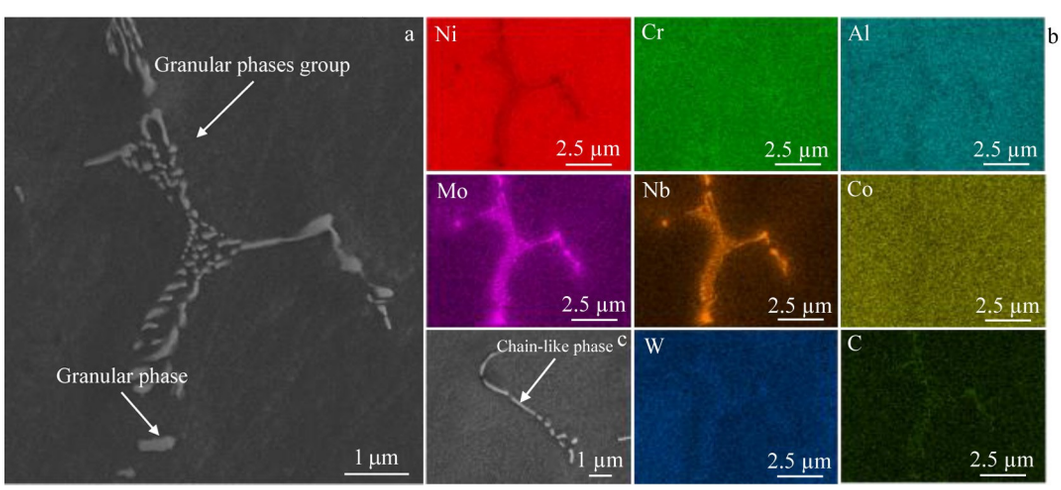

Fig.6 SEM images of precipitated phases (a, c) and corresponding EDS element mappings (b)

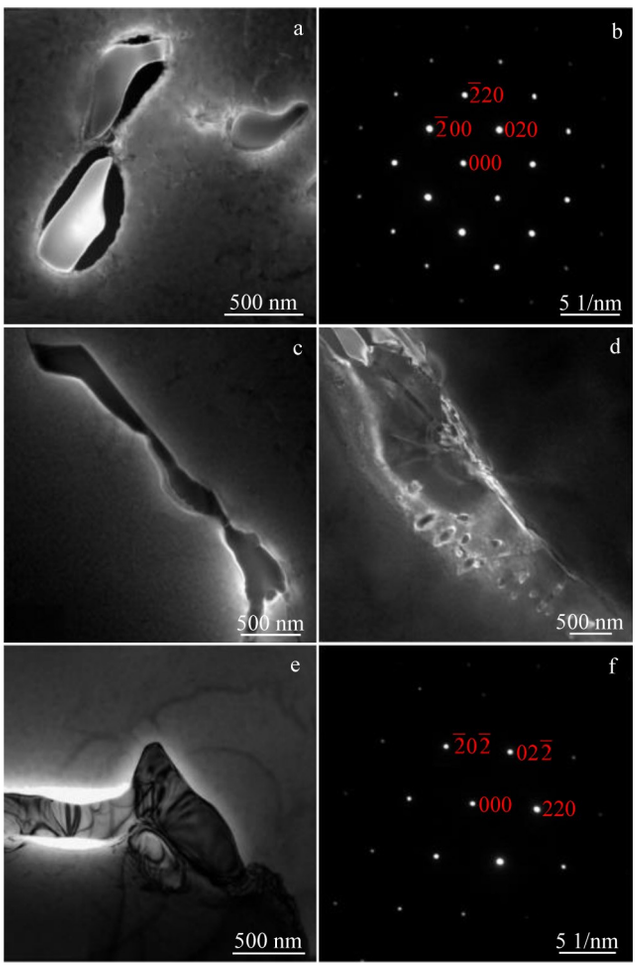

Fig.7 TEM images of precipitated phases (a, c – e); SAED patterns corresponding to Fig.7a (b) and Fig.7e (f)

liquation cracks of the welded joints are mainly initiated in the HAZ. During the welding heating process, the components of the low-melting-point precipitate in the HAZ are liquefied, forming a low-melting-point liquid film between the grains. When the tensile stress generated during the cooling process is greater than the surface tension of the liquid film, it will cause the initiation of liquation cracks[18,33]. Most of the liquation cracks are small and zigzag, and the constitutional liquation of the precipitated phase can be observed near the cracks. The liquation cracks and their element mappings are shown in Fig.9, and the liquation of the carbides near the cracks can be observed.

The total crack length (TCL) of joints with six groove shapes was measured and averaged. The results are shown in Table 3. The joints with grooves G3, G4, and G5 have more cracks, while the TCLs of joints with grooves G2 and G6 are the smallest. It has been found that the aspect ratio (defined as depth divided by the width) of the welded joint has a greater influence on the welding results[27], and the data in Table 3 show that welding cracks are less frequent for melt pool shapes with aspect ratios between 0.3 and 0.5. Combining the element segregation data in Fig.4, it can be known that joints with aspect ratios of 0.3 to 0.5 have lower element segregation.

3.3 Influence of aspect ratio of grooves

The EBSD results for the joints with six groove shapes are shown in Fig.10, where the welding cracks are initiated at the high-angle grain boundaries. The comparison between the IPF and KAM maps shows that the joints with aspect ratios of 0.3 to 0.5 have fewer fine grains and a more homogeneous geometrically necessary dislocation. The KAM map reflects that the distribution of geometrically necessary dislocations within a grain is due to the local misorientation, and the

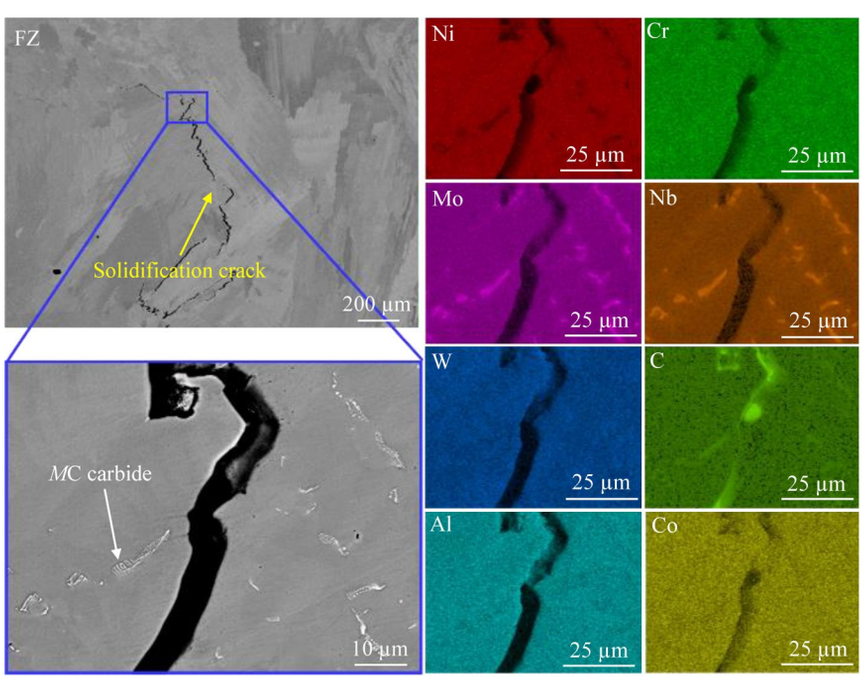

Fig.8 SEM images and EDS element mappings of solidification cracks

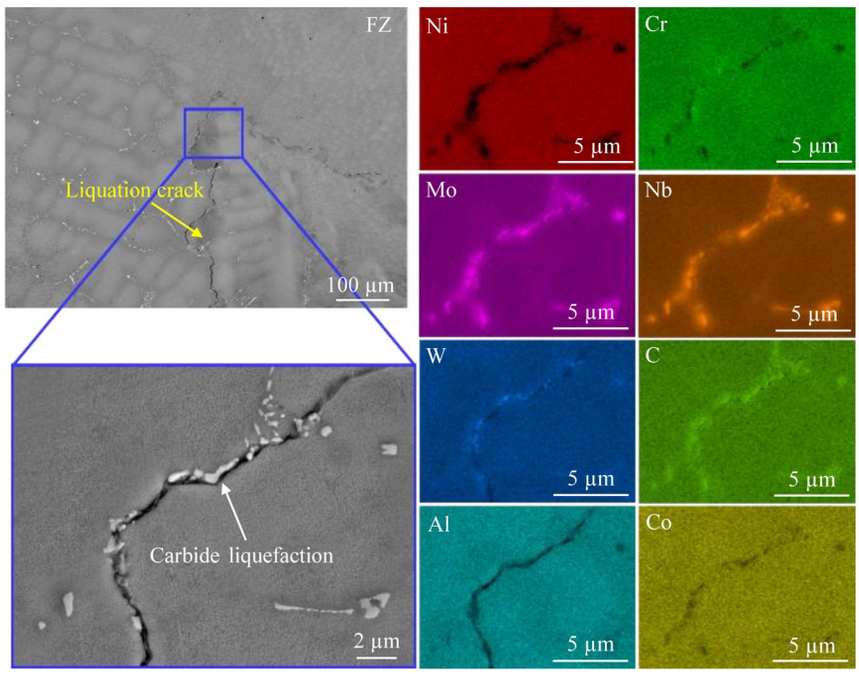

Fig.9 SEM images and EDS element mappings of liquation cracks

Table 3 TCL and aspect ratio of six joints

Groove	G1	G2	G3	G4	G5	G6
TCL/μm	5586	1693	7758	6621	9335	3930
Aspect ratio	0.25	0.5	0.75	1	0.6	0.375

density of geometrically necessary dislocations can indirectly reflect the residual stress in the joint. Welding cracks are mostly caused by residual stress. The geometrically necessary dislocation density must be high around the welding cracks. Therefore, the residual stress distribution of the joint with a moderate aspect ratio is also more homogeneous.

The tensile results of joints with six kinds of groove shapes at 800 °C are shown in Fig. 11. It can be observed that the tensile strength is related to the TCL, and the TCL is related to the aspect ratio of the grooves. The TCL is the smallest, and the tensile strength is the highest when the groove aspect ratio is 0.2 – 0.5. The tensile fracture morphologies are shown in Fig. 12. All fracture morphologies of six grooves have the characteristics of an intergranular fracture. Secondary cracks are observed in each fracture, and most are located at the bottom of the FZ, which are judged to be liquation cracks. In addition, several dimples are found at the fracture of joints with grooves G2 and G5, and it is judged that the fracture mode of these two joints is a brittle-ductile mixed fracture. Therefore, the fracture mode of the joint with the groove aspect ratio of 0.2–0.5 is a mixed fracture, and the others are brittle fractures.

The groove shape mainly affects the welding quality by affecting the stress state, crystallization condition, and heat distribution of the joint. The generation of cracks in welded joints is mainly related to the thermal stress in the welding process, and the stress change in the welding process is shown in Fig. 13[34]. Taking the longitudinal stress σ_x as an example, the temperature of the weld center is the highest during welding, and the metal of the weld is still in a molten state, σ_x= 0. Then, the metal around the weld is subjected to thermal expansion, which provides tensile stress, and the weld is under compressive stress. As the welding process proceeds, the weld is gradually cooled down, the center of the weld turns to tensile stress, while the metal on both sides of the weld is subjected to compressive stress, which is the distribution of residual stress in the joint after welding.

The shape of the groove mainly affects the distribution of residual stress by changing the constraint state of the weld metal. The deeper the groove depth, the larger the tensile stress at the weld center, thereby deteriorating the metal's weldability. In the case of a certain depth, increasing the width of the groove can alleviate the tensile stress in the weld center. However, if the groove is too wide, multi-pass welding is required, which will also initiate welding cracks.

In TIG welding, the molten pool temperature reaches about 1800 °C, the liquid metal is in a superheated state, and there are few spontaneous nucleation particles. Therefore, most of the crystal nuclei attach to the semi-melted grains of the BM and grow in the form of columnar crystals to the center of the weld, which is also confirmed by the EBSD results in Fig. 10. Some recrystallized grains are found at the edge of the FZ. It is considered that during the cooling process of the weld, the columnar crystals at the boundary of the FZ grow towards the center, and some tensile stresses already exist in the dendritic crystals that take the lead in solidification, providing the energy required for nucleation and promoting the formation of these recrystallized grains, as shown in Fig. 14. As the weld continues to cool, the temperature of the weld center

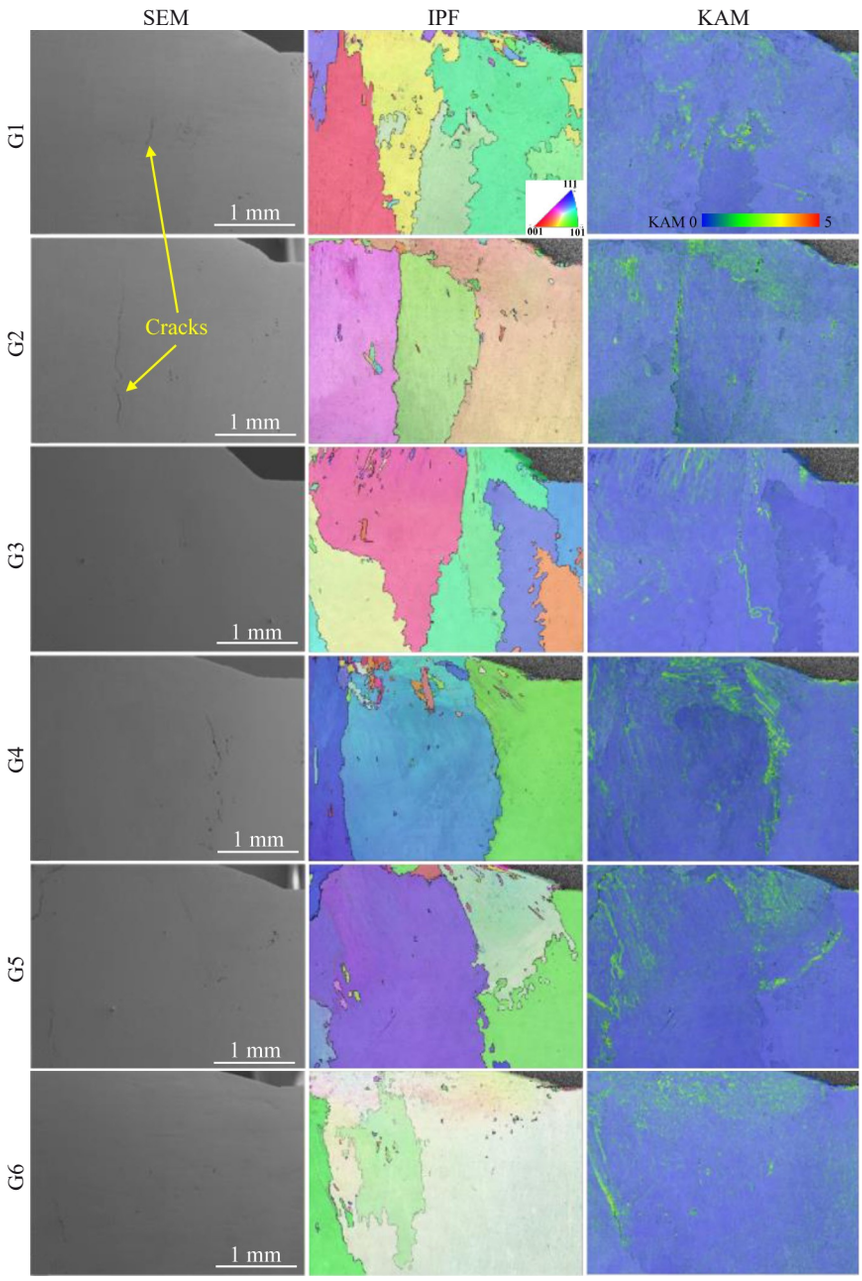

Fig.10 SEM images, IPFs, and KAM maps of joints with six kinds of groove shapes

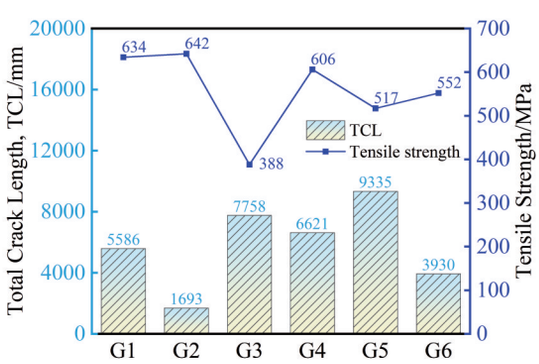

Fig.11 TCL of joints with six kinds of groove shapes and corresponding tensile strength at 800 °C

decreases, the nucleation condition becomes worse, leading to the formation of finer equiaxed crystals in the weld center. Joints with high residual stress, such as those in the six cases mentioned, tend to have finer crystals.

The test results show that joints with grooves G3 and G4 have a high degree of stress concentration and more fine crystals. The grain boundary is the final solidification part of the weld, and it is also the weakest part of the superalloy. With the solidification of the weld, more residual stress accumulates at the grain boundary. When the residual stress $\sigma_R > 2\gamma_{sl}/h$, where γ_{sl} is the surface tension of the solid-liquid interface and h is the thickness of the liquid film, the cracks are initiated[35].

In addition, the distribution of heat in the groove during

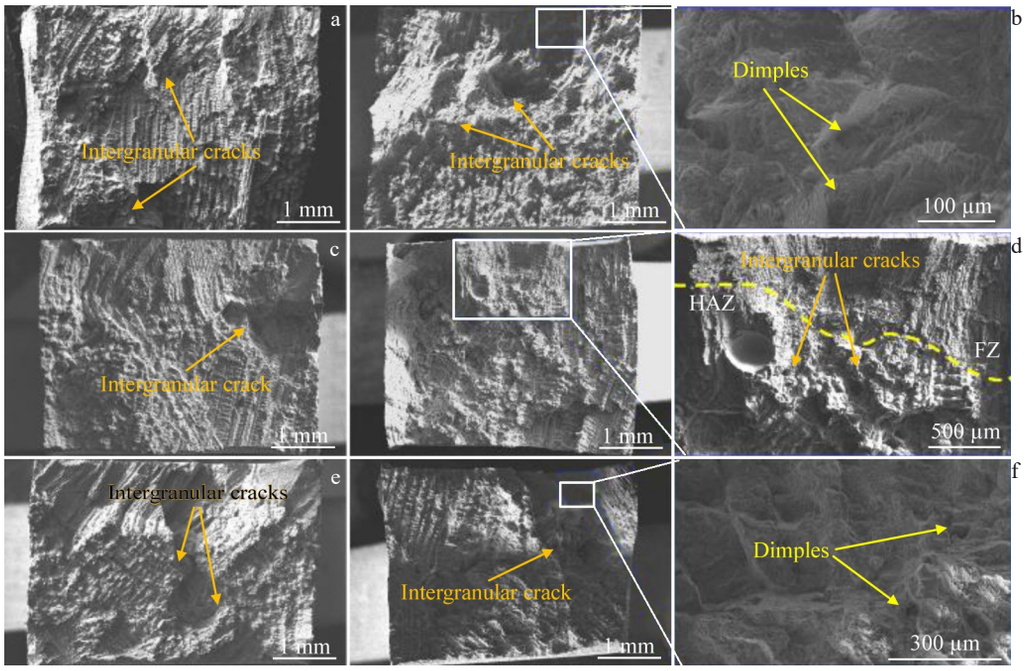

Fig.12 Fracture morphologies of joints with six kinds of groove shapes: (a) G1; (b) G2; (c) G3; (d) G4; (e) G5; (f) G6

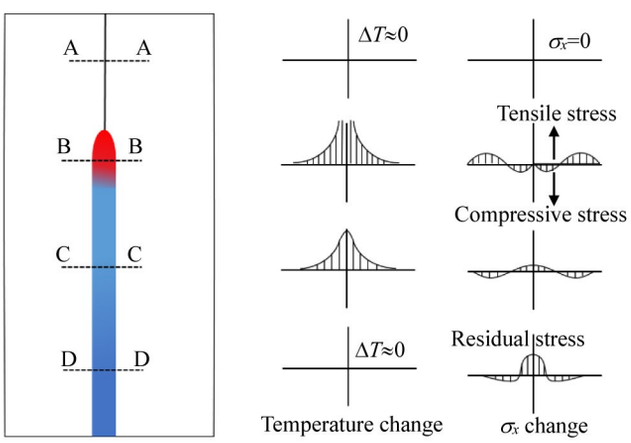

Fig.13 Schematic diagrams of residual stress formation during welding progress[34]

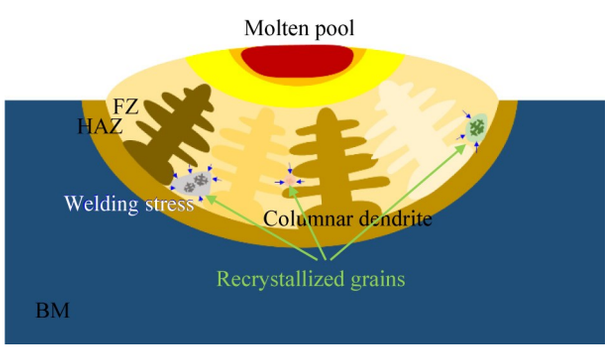

Fig.14 Schematic diagram of recrystallized grain formation in the FZ

welding is also crucial to the welding results, and there are mainly Gaussian heat source models, double ellipsoid heat source models, and generalized double ellipsoid models for welding heat sources[36–38]. Taking the Gaussian heat source as an example, the heat energy transferred into the base material through a unit area per unit time during welding, i. e., heat flow density q, is calculated as follows[36]:

$$q(r)=q_{\mathrm{m}}\mathrm{e}^{-Kr^2} \quad (2)$$

where r is the distance from a point in the area covered by the arc to the center of the heat source, q_{m} is the maximum heat flux density, and K is the heat source concentration factor. In the places below and near the heat source, the arc in the same plane transmits the maximum heat energy to the BM. As the groove depth gradually increases, the rate of heat drop slows down, the degree of elastic deformation of the metal near the weld increases, and the thermal stress generated during the cooling process increases. The superalloy cracks when the thermal stress exceeds the limit that the liquid film can withstand.

4 Conclusions

1) When the welding wires with a similar composition to the K4951 superalloy are used to weld the K4951 superalloy, a joint with fewer defects can be obtained, where nano-scale *M*C carbides are primarily precipitated.

2) The aspect ratio of the grooves or casting defects has a great influence on the welding quality. When this ratio falls within the range of 0.2 to 0.5, several characteristics of the joint are affected: the degree of element segregation decreases, the fine crystal content reduces, the TCL shortens, the tensile strength improves, and the fracture mode exhibits a brittle-ductile mixed behavior.

3) The grooves or casting defects mainly affect the welding results through the restraint state, crystallization conditions,

and heat distribution. When the groove depth exceeds 3 mm or the width exceeds 5 mm, the joint becomes susceptible to incomplete fusion defects, thus deteriorating the weldability of the superalloy.

References

1 Grant B M B, Francis E M, Quinta Da Fonseca J *et al. Acta Materialia*[J], 2012, 60(19): 6829
2 Sato J, Omori T, Oikawa K *et al. Science*[J], 2006, 312(5770): 90
3 Martín Ó, De T P, San J M. *Materials Science and Engineering A*[J], 2017, 688: 309
4 Cui L Q, Yu J J, Liu J L *et al. Journal of Alloys and Compounds*[J], 2019, 773: 250
5 Yu J J, Lian Z W, Chu Z K *et al. Materials Science and Engineering A*[J], 2010, 527(7): 1896
6 Yang Y H, Yu J J, Sun X F *et al. Materials Characterization*[J], 2012, 66: 30
7 Lian Z W, Yu J J, Sun X F *et al. Materials Science and Engineering A*[J], 2008, 489(1): 227
8 Zhou P J, Yu J J, Sun X F *et al. Transactions of Nonferrous Metals Society of China*[J], 2012, 22(7): 1594
9 Wang Guan, Song Wei, Liang Jingjing *et al. Rare Metal Materials and Engineering*[J], 2024, 53(3): 787 (in Chinese)
10 Zhang J L, Zhang Z, Zhao Z H *et al. Materials Letters*[J], 2019, 235: 57
11 Zhang X Y, Wang S Y, Liu H *et al. Materials Science and Engineering A*[J], 2024, 903: 146696
12 Wen M Y, Sun Y, Yu J J *et al. Journal of Materials Science & Technology*[J], 2021, 78: 260
13 Wang Shiyang Liu Shiwei, Hou Xingyu *et al. Transactions of the China Welding Institution*[J], 2023, 44(3): 31 (in Chinese)
14 Sun Yuan, Qin Xindong, Wang Shiyang *et al. Chinese Journal of Engineering*[J], 2024, 46(6): 1065 (in Chinese)
15 Catchpole S S, Aboulkhair N, Parry L *et al. Additive Manufacturing*[J], 2017, 15: 113
16 Prager M, Shira C S. *Welding Research Council Bulletin*[J], 1968(128): 1
17 Lee S J, Seo S M, Chun E J. *Materials Chemistry and Physics*[J], 2024, 316: 129147
18 Ojo O A, Richards N L, Chaturvedi M C. *Scripta Materialia*[J], 2004, 50(5): 641
19 Li Y, Wang J, Han E H *et al. Journal of Materials Science & Technology*[J], 2019, 35(4): 545
20 Xie J L, Ma Y C, Xing W W*et al. Welding in the World*[J], 2018, 62(3): 471
21 Chen J W, Salvati E, Uzun F *et al. Journal of Manufacturing Processes*[J], 2020, 53: 190
22 Ojo O A, Richards N L, Chaturvedi M C. *Scripta Materialia*[J], 2004, 51(7): 683
23 Ariaseta A, Khan A K, Andersson J *et al. Materials Characterization*[J], 2023, 204: 113178
24 Ye X, Hua X M, Wang M *et al. Journal of Materials Processing Technology*[J], 2015, 222: 381
25 Wang Z M, Gui Z X, Wu J W *et al. Journal of Manufacturing Processes*[J], 2023, 89: 338
26 Zhong M L, Sun H Q, Liu W J *et al. Scripta Materialia*[J], 2005, 53(2): 159
27 Rush M T, Colegrove P A, Zhang Z *et al. Journal of Materials Processing Technology*[J], 2012, 212(1): 188
28 Richards N L, Nakkalil R, Chaturvedi M C. *Metallurgical and Materials Transactions A*[J], 1994, 25(8): 1733
29 Gremaud M, Carrard M, Kurz W. *Acta Metallurgica et Materialia*[J], 1990, 38(12): 2587
30 Shulga A V. *Journal of Alloys and Compounds*[J], 2007, 436(1): 155
31 Lian Zhanwei, Yu Jinjiang, Sun Xiaofeng *et al. Rare Metal Materials and Engineering*[J], 2008, 37(5): 798 (in Chinese)
32 Harrison N J, Todd I, Mumtaz K. *Acta Materialia*[J], 2015, 94: 59
33 Zhang Z, Zhao Y, Shan J *et al. Materials Science and Engineering A*[J], 2021, 823: 141678
34 Masubuchi K. *Analysis of Welded Structures*[M]. Oxford: Pergamon Press, 1980: 148
35 Miller W A, Chadwick G A. *Acta Materialia*[J], 1967, 15(4): 607
36 Pavelic V, Tanbakuchi R, Uyehara O A *et al. Welding Journal*[J], 1969, 48(7): S295
37 Goldak J, Chakravarti A, Bibby M. *Metallurgical Transactions B-Process Metallurgy*[J], 1984, 15(2): 299
38 Farias R M, Teixeira P R F, Vilarinho L O. *International Journal of Thermal Sciences*[J], 2022, 179: 107593

铸造缺陷对一种高温合金可焊性的影响

储清泉[1,2]，侯星宇[1]，程　印[1]，秦　建[3]，王诗洋[1]，孙　元[1]，孙晓峰[1]

(1. 中国科学院 金属研究所 师昌绪先进材料创新中心，辽宁 沈阳 110016)

(2. 中国科学技术大学 材料科学与工程学院，辽宁 沈阳 110016)

(3. 中国机械总院集团郑州机械研究所有限公司 高性能新型焊接材料全国重点实验室，河南 郑州 450052)

摘　要：使用钨极氩弧焊（TIG）方法对预制不同深度与宽度的“U”形槽的K4951高温合金进行焊接，探讨了铸造缺陷对合金可焊性的影响。采用光学显微镜、扫描电子显微镜、透射电子显微镜和能谱仪对焊后接头进行观察，并对接头微观结构、裂纹形态以及析出相进行分析。结果表明，铸造缺陷的尺寸对K4951合金的可焊性有很大影响，缺陷深度大于2 mm会导致裂纹快速扩展，而较宽的缺陷则会缓和裂纹的扩展进程。接头焊缝中观察到元素偏析和析出相（如*M*C碳化物）的形成，这与焊接裂纹的萌生相关。另外，凹槽深宽比在0.2至0.5之间时，裂纹形成倾向最小，接头抗拉伸强度高，接头高温拉伸后呈脆性与韧性混合断裂模式。

关键词：铸造缺陷；K4951；TIG；可焊性

作者简介：储清泉，男，2000年生，硕士，中国科学技术大学材料科学与工程学院，辽宁 沈阳 110016，E-mail：qqchu22s@imr.ac.cn